Citation: Molecular Therapy—Nucleic Acids (2016) 5, e363; doi:10.1038/mtna.2016.68
Official journal of the American Society of Gene & Cell Therapy
www.nature.com/mtna

Lipid Nanoparticle Delivery of siRNA to Osteocytes Leads to Effective Silencing of *SOST* and Inhibition of Sclerostin *In Vivo*

Genc Basha[1], Mina Ordobadi[1], Wilder R Scott[2], Andrew Cottle[1], Yan Liu[1], Haitang Wang[1] and Pieter R Cullis[1]

Sclerostin is a protein secreted by osteocytes that is encoded by the *SOST* gene; it decreases bone formation by reducing osteoblast differentiation through inhibition of the Wnt signaling pathway. Silencing the *SOST* gene using RNA interference (RNAi) could therefore be an effective way to treat osteoporosis. Here, we investigate the utility of lipid nanoparticle (LNP) formulations of siRNA to silence the *SOST* gene *in vitro* and *in vivo*. It is shown that primary mouse embryonic fibroblasts (MEF) provide a useful model system in which the *SOST* gene can be induced by incubation in osteogenic media, allowing development of optimized *SOST* siRNA for silencing the *SOST* gene. Incubation of MEF cells with LNP containing optimized *SOST* siRNA produced significant, prolonged knockdown of the induced *SOST* gene *in vitro*, which was associated with an increase in osteogenic markers. Intravenous (i.v.) administration of LNP containing *SOST* siRNA to mice showed significant accumulation of LNP in osteocytes in compact bone, depletion of *SOST* mRNA and subsequent reduction of circulating sclerostin protein, establishing the potential utility for LNP siRNA systems to promote bone formation.

Molecular Therapy—Nucleic Acids (2016) **5**, e363; doi:10.1038/mtna.2016.68; published online 13 September 2016
Subject Category: siRNAs, shRNAs and miRNAs Nanoparticles

Introduction

Treatment of progressive bone diseases such as osteoporosis is a challenging problem and a significant unmet clinical need. Osteoporosis is a systemic skeletal disorder characterized by low bone mass and a progressive microarchitectural deterioration of bone tissue, leading to an increase in bone fragility and ultimately a susceptibility to bone fractures.[1] Given the clear link between modulation of the Wnt/β-catenin signaling pathway and certain human diseases, there has been an increasing interest in clarifying the role of proteins regulating the Wnt/β-catenin pathway and bone mass regulation.[2] Sclerostin, a protein secreted largely by osteocytes, is a negative regulator of osteoblast differentiation and functions by inhibiting the Wnt and bone morphogenetic protein signaling pathways that are critical for osteoblast proliferation and activity.[3–5] Humans with inherited sclerostin deficiency (sclerosteosis or van Buchem disease) have increased bone mass and are resistant to fracture.[5,6] Importantly, in menopausal women with low bone mass, administration of antibodies targeting sclerostin was associated with increased bone mineral density, bone formation, and decreased bone resorption.[6] This, coupled with the fact that sclerostin is the only pathway modulator that is highly selective for bone, with its secretion being restricted to osteocytes, suggests that blocking the function of the Wnt antagonist sclerostin could result in new therapeutics to increase bone formation.

Recently, RNA interference (RNAi), has emerged as a novel therapeutic modality, potentially able to silence any desired gene. Impressive preclinical results have been achieved using RNAi to treat metabolic, degenerative, and genetic disorders, as well as cancer and inflammation.[6,7] Further, new insights into bone biology are producing new therapeutic targets for bone pathologies. For example, RNAi-based therapies targeting genes that are known to negatively regulate bone formation, such as the *SOST* gene, could lead to treatments for diseases exhibiting impaired bone formation. This will require the development and optimization of efficient delivery methods to bone tissue. The major obstacle for developing siRNA for therapeutic applications is the need for effective delivery with clinically acceptable formulations and acceptable routes of administration. This is particularly true for the delivery to compact bone, which exhibits an intrinsically poor drug penetration and vascular perfusion. To date, formulation of nucleic acid therapeutics in lipid nanoparticles (LNPs) represents one of the most effective strategies for *in vivo* delivery, particularly for the liver.[7,8] In this study, we investigate first whether expression of the *SOST* gene can be effectively inhibited *in vitro* (using a surrogate primary stem cell model) employing an siRNA-mediated approach delivered by LNPs. Second, we assess the functional effect of *SOST* knockdown on bone osteogenic markers *in vitro* . Finally, we demonstrate effective delivery of LNP-siRNAs to osteocytes in compact bone and consequent silencing of the *SOST* gene *in vivo* following systemic administration of LNP-siRNA-*SOST*.

[1]NanoMedicines Research Group, Department of Biochemistry and Molecular Biology, Life Sciences Institute, University of British Columbia, Vancouver, British Columbia, Canada; [2]Department of Cellular and Physiological Sciences, Biomedical Research Centre, University of British Columbia, Vancouver, British Columbia, Canada. Correspondence: G Basha, NanoMedicines Research Group, Department of Biochemistry and Molecular Biology, Life Sciences Institute, University of British Columbia, 2350 Health Sciences Mall, Vancouver, British Columbia, Canada V6T 1Z3. E-mail: gbasha@mail.ubc.ca
Key words: bone formation; lipid nanoparticles; sclerostin; siRNA
Received 16 June 2016; accepted 19 July 2016; published online 13 September 2016. doi:10.1038/mtna.2016.68

Results

Characterization of lipid nanoparticles

Particle size was 36.93 nm (PDI = 0.049) and 37.88 nm (PDI = 0.044) for *siSOST* and siLuciferase particles, respectively. Encapsulation efficiency measured using Quant-iT Ribogreen RNA assay was greater than 90% for both types of LNP (91.87 ± 0.4976 and 93.99 ± 1.405% for *siSOST* and siLuciferase particles, respectively). Since the pKa of the ionizable cationic lipid component of the particles, DLin-MC3-DMA, is 6.44, the particles have a near neutral surface charge at a physiological pH of 7.4.

In vitro SOST induction is associated with upregulation of bone osteogenic markers

Primary mouse embryonic fibroblasts (MEFs) were isolated and cultured for 2 weeks in Dulbecco's Modified Eagle's Medium (DMEM) or in osteogenic medium (OM). During this time, MEFs were harvested every other day and qRT-PCR analysis was carried out using *SOST*-specific primers. MEFs treated with OM generated increased *SOST* transcripts that were detectable after 3 days of treatment and increased by up to 100-fold after 2 weeks incubation time (**Figure 1a**). However, cells incubated with DMEM produced only background levels of *SOST* transcripts after 2 weeks incubation. Sclerostin protein expression was also measured during MEF culture in DMEM or OM using western blot analysis. It was observed that cells incubated with OM exhibited significantly higher amounts of sclerostin protein after 1 week incubation with further increases after 2 weeks (**Figure 1b**,**c**). To confirm the osteogenic character of the MEFs treated with OM, we also examined the expression of *Alp*, an early marker of osteogenic differentiation. Osteogenic stimulation generated a large (up to 1,600-fold) increase in *Alp* transcripts over 2 weeks of incubation as compared to cells treated with DMEM (**Figure 1d**). This increase was also confirmed using an enzymatic assay for ALP in cells cultured in DMEM or OM over 2 weeks (**Figure 1e**). After 1 and 2 weeks, the intensity of alkaline phosphatase staining was significantly increased as compared to cells treated with DMEM (**Figure 1f**). To further confirm the osteogenic identity of OM-treated MEFs, we also examined the expression of additional early (*Sp7* and *Runx2*) and late-stage (*Bsp*) osteogenic markers. It was observed that all three genes were differentially but significantly upregulated when MEFs were treated with OM, compared to those treated with DMEM (**Figure 1g–i**). Taken together, the data indicate that the MEF system incubated in OM provides an *in vitro* system where *SOST* is expressed at significant levels following 1 week of incubation. In addition, the increased expression of early and late osteogenic markers accompanying increased *SOST* expression levels suggest that MEFs could be utilized as an *in vitro* system to assess the impact of *SOST* downregulation on bone osteogenic marker genes.

Mouse embryonic fibroblasts exhibit substantial uptake of LNP-siRNA *in vitro*

The second set of experiments were aimed at assessing the ability of primary MEF cells to accumulate LNP siRNA systems. MEFs were incubated with DiI-labeled LNP containing Quasar-570-labeled siRNA. Cellular uptake of LNPs and associated siRNA was monitored for 15, 30, 60, and 120 minutes by measuring the intensity of the DiI and Quasar-570 fluorescence in MEFs using live confocal microscopy (**Figure 2**). A high uptake efficiency was observed at all incubation times, as indicated by the intracellular accumulation of siRNA (red color, **Figure 2a**) or LNP (green color, **Figure 2b**). siRNA in the MEFs was detected as early as 15 minutes following incubation. The intracellular delivery of dye labeled-siRNA and LNP increased over time as detected by the amount and intensity of the fluorescence. Also, based on the pattern of fluorescence and its intensity, a good correlation was observed between siRNA and LNP uptake by MEFs, indicating that these LNP systems can deliver siRNA quickly and efficiently to the cell without affecting cell viability. Quantification of the fluorescence further demonstrated a significant uptake of LNP-siRNAs by MEFs within 15 minutes following incubation and a fairly good correlation between LNPs and siRNAs (**Figure 2c**). To better quantify the intracellular delivery of LNP-siRNA systems in MEFs, a flow cytometry-based assay was carried out. As the fluorescence intensity of Alexa647-labeled siRNA can be sensitive to breakdown by nucleases, the relative levels of uptake were measured by having both LNPs and siRNA labeled with DiO and Alexa647 respectively. Cellular uptake of siRNA and LNP lipid was monitored over 48 hours by measuring the fluorescence intensity of Alexa647 and DiO in MEFs (**Figure 2d**). For all incubation times tested, significantly more uptake of LNP-siRNA was observed relative to free-siRNA, confirming that delivery with LNPs is absolutely necessary to protect siRNA from degradation and maximize intracellular transfer of the payload. A good correlation of LNP and siRNA was also observed as fluorescence of both LNPs and siRNAs diminished overtime presumably due to siRNA translocation in to the cytosol while LNPs were metabolized in the cell. As demonstrated by Alexa647 fluorescence, free-siRNA is degraded within hours in the cell cytoplasm.

siRNA screening to identify the anti-*SOST* duplex that mediates optimized knockdown of the *SOST* gene

MEFs were transfected with the fluorescently-labeled transfection control duplex TYE 563-red. For convenience, the RNAiMAX transfection reagent (Life Technologies) was used in these studies. Cells were examined at 24 hours after transfection. Microscopy revealed high efficiency of transfection of MEFs to about 70 or 80% following incubation with 10 or 30 nmol/l TYE 563-labeled siRNA respectively (**Supplementary Figure S1a**). MEFs pretreated with OM were also transfected with six siRNA duplexes (A through F), including the *Hprt* positive control and a scrambled siRNA as a negative control, at doses of 3, 10, and 30 nmol/l (**Supplementary Table S1**). Relative mRNA levels were measured using qRT-PCR at 48 hours post-transfection. Data were normalized against internal *Hprt* or *Tbp* (for the positive control) housekeeping genes considering the siCtrl as baseline 100%. It was observed that sequence B and C could significantly reduce the expression of *SOST* at doses of 3, 10, and 30 nmol/l (**Supplementary Figure S1b**). Sequence C in particular, produced a 70 to 75% knockdown of *SOST* when treated at 10 and 30 nmol/l, respectively, similar to siRNA targeting *Hprt*, a positive control. Sequence A (not shown) and the rest of duplexes did not induce significant downregulation of the target gene. It was concluded that

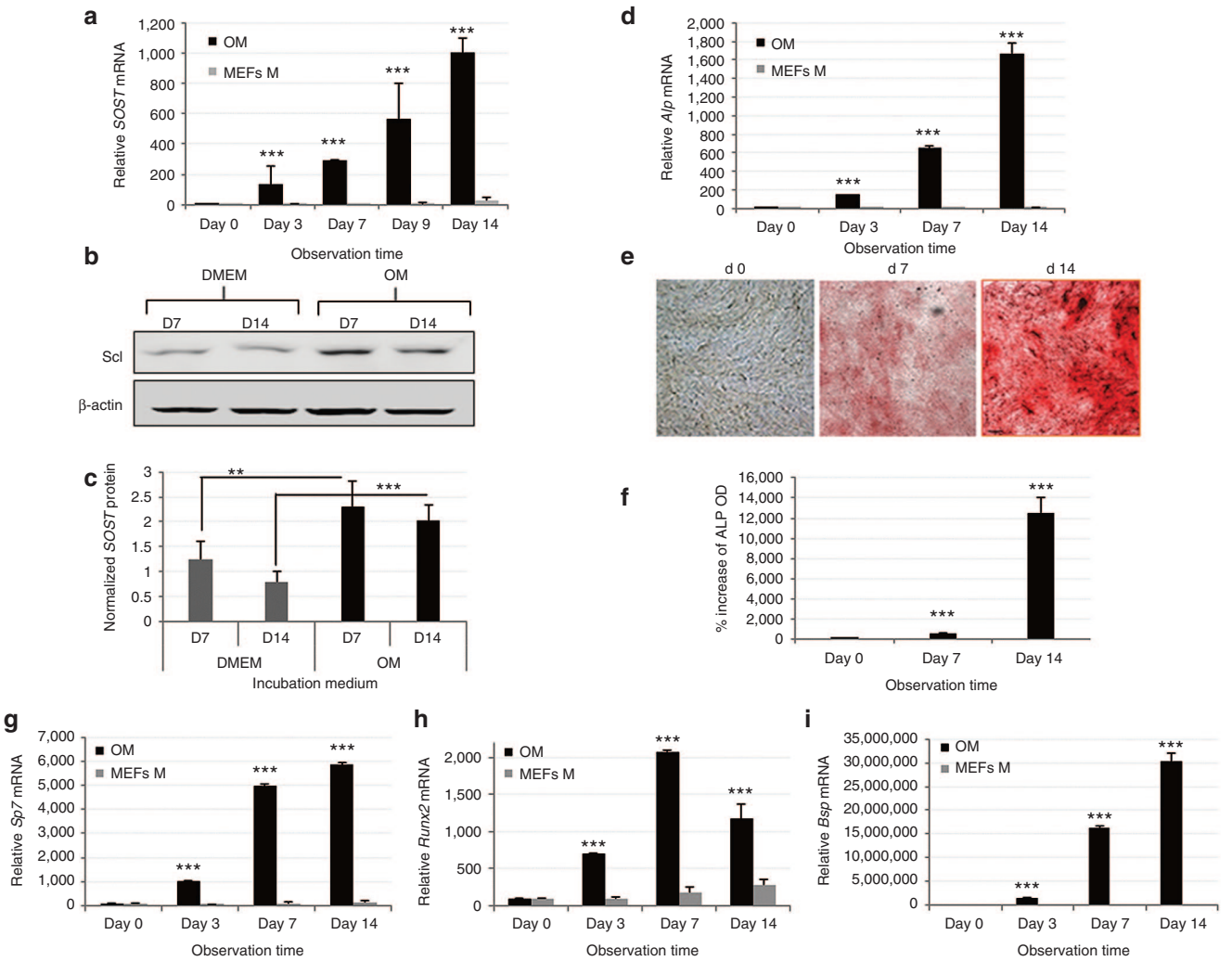

Figure 1 ***In vitro SOST* induction and effect on bone osteogenic markers**. Mouse embryonic fibroblasts (MEFs) were plated in 12-well plates at appropriate density to achieve maximum confluence. Cells were incubated in DMEM or OM and total RNA was extracted to measure (**a**) *SOST*, (**d**) *Alp*, (**g**) *Sp7*, (**h**), *RunX2*, and (**i**) *Bsp* mRNA at time points indicated. Bar graphs represent expression of the target mRNA relative to the *Hprt* house keeping gene with or without OM. mRNA values at day 0 are considered 100%. Data are shown as mean ± SD of triplicate wells and are representative of at least three experiments. (**b**) Protein was extracted from cell lysates and the expression of sclerostin was determined in protein extracts using SDS-polyacrylamide gel electrophoresis and western blotting followed by anti-sclerostin antibody staining. Blots are representative of multiple experiments. (**c**) Sclerostin expression was assessed over time following incubation of MEFs with DMEM or OM and the intensity of the bands were quantified. Bar graphs shown as mean ± SD represent data obtained from multiple experiments. (**e**) Alkaline activity was assessed following staining of MEFs incubated in DMEM or OM in triplicate plates. Data represent not less than 3 images captured with a 200× objective. (**f**) Alkaline phosphatase expression was also quantified. Bar graphs shown as mean ± SD represent data obtained from at least three images and multiple areas captured from each image (**$P < 0.01$; ***$P < 0.001$).

sequence C was the most effective duplex to be used to assess *SOST* knockdown and its effect in bone osteogenic markers. As siRNA duplexes are susceptible to degradation *in vivo*, sequence C was chemically modified by adding 2′ O-methyl bases that block exonuclease activity and improves resistance to nucleases *in vivo* (stealth siRNA). To assess the efficacy of the modified duplex and rule out toxicity, MEFs were plated and treated with the modified (Stealth) and nonmodified (standard) siRNA using the same transfection method, and *SOST* mRNA was measured using qRT-PCR. It was observed that Stealth *SOST*-siRNA showed similar efficacy to unmodified duplex, producing 80% knockdown of *SOST* without detectable cell toxicity (**Supplementary Figure S2**).

Next, we examined the effect of anti-*SOST*-siRNA (*siSOST*) delivered in LNP. MEFs were plated and treated with LNP siLuc as control (siCtrl) or LNP *siSOST* for 3 and 7 days. Following treatment, *SOST*-mRNA and *Tbp* housekeeping gene transcripts were measured using qRT-PCR analysis. *siSOST*-treated MEFs exhibited significant downregulation relative to siLuc controls of *SOST*-mRNA for all three doses tested, yielding 60, 70, and 80% knockdown after 3 days treatment, while the housekeeping *Tbp* gene expression remained constant at all doses tested (**Figure 3a**,**b**). In addition, 7 days of treatment reduced *SOST* expression in a dose dependent manner leading to 90% downregulation following treatment with 10 µg/ml siRNA, without affecting *Tbp*

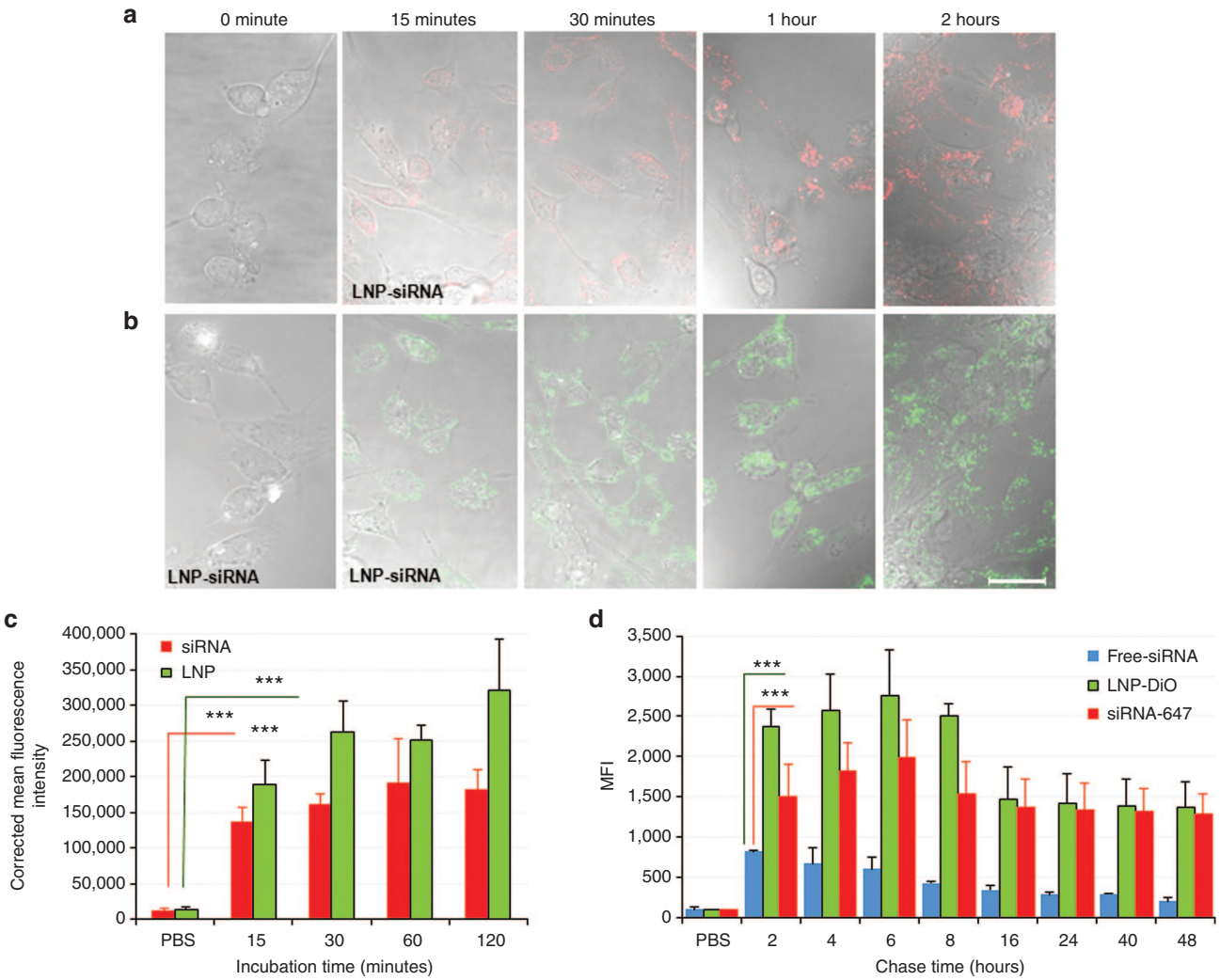

Figure 2 Visualization and quantification of effective uptake of LNP-siRNA by MEFs. Mouse embryonic fibroblasts (MEFs) were seeded in glass bottom culture dishes and when 80% confluent, (**a**) Quasar570-labeled LNP-siRNA (red) and (**b**) DiI-labeled LNP-siRNA (green) were added to the cells at 5 µg/ml to monitor the cellular uptake of siRNA and LNPs. DMEM was replaced with phenol-free medium prior to live cell imaging, and live cells were analyzed in a Leica confocal microscope at time points indicated. A minimum of three images were examined for each time point. Scale bar = 5µm. (**c**) Intracellular fluorescence was also quantified. Bar graphs shown as mean ± SD ($n = 3$) represent data obtained from two different experiments ***$P < 0.001$. (**d**) MEFs were incubated with 2 µg/ml LNP (DiO green)-siRNA (Alexa647 far red) and fluorescence intensity was assessed at time points indicated using flow cytometry. The bar graphs depict percent increase (mean ± SD, $n = 3$) of mean fluorescence intensity over time relative to PBS-treated controls and free siRNA. Data are representative of two different experiments performed in triplicate (***$P < 0.001$).

(**Figure 3c**,**d**). Taken together, the data indicate that LNPs can efficiently deliver siRNA to primary MEFs resulting in significant *SOST* gene knockdown.

siRNA-mediated *SOST* knockdown modulates differentiation of MEFs

To determine the anabolic effect of RNAi-mediated *SOST* knockdown, we measured the expression of early and late markers of osteogenic differentiation. MEFs were treated with *siSOST* or siCtrl, harvested after 3 and 7 days of incubation and bone osteogenic markers were measured using qRT-PCR analysis. It was observed that MEFs treated with *siSOST* generated increased *Alp* transcripts compared with cells treated with siCtrl and that this increase was dose dependent. The *Alp* increase was more evident at 5 and 10 µg/ml doses (**Figure 4a**). To confirm the osteogenic identity of this transformation of MEFs, we also examined the expression of additional early and late-stage osteogenic markers (**Supplementary Table S2**). Except for *Pthr1*, which remained unchanged, *Coll1A1/2*, Osteocalcin (*Ocn*) and Osterix (OSX) were all differentially upregulated following treatment with *siSOST* compared with siCtrl, and this upregulation was generally dose dependent (**Supplementary Figure S3**). Seven days of treatment did not increase the expression of bone osteogenic genes. The key regulators of bone formation *Alp*, *Coll1A2*, and *Ocn* however, remained elevated compared to siCtrl (**Figure 4b**), whereas other genes exhibited minor downregulation (**Supplementary Figure S3**). Cathepsin K (involved in bone resorption) gene expression increased after 3 days of treatment but normalized by day 7. Finally,

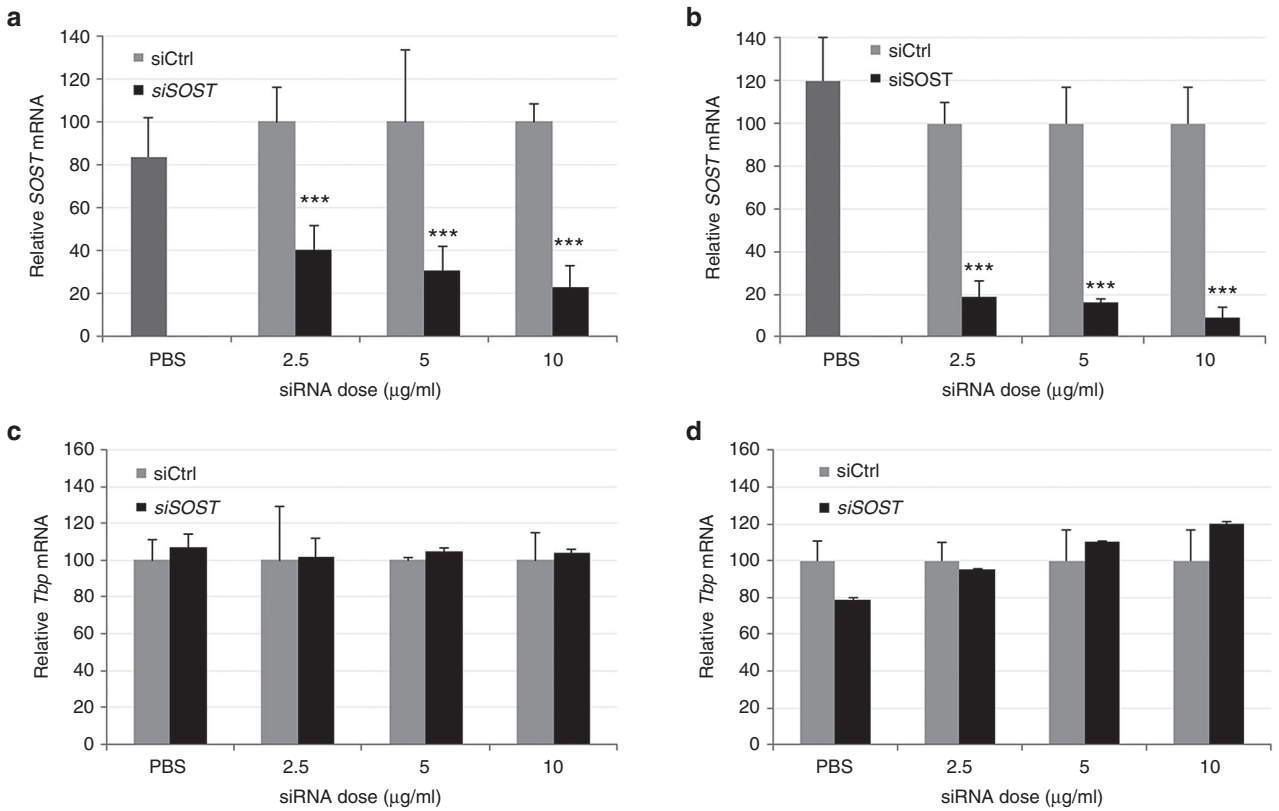

Figure 3 siRNA-mediated knockdown of *SOST* gene *in vitro* is gene specific. To investigate the siRNA-mediated knockdown, mouse embryonic fibroblasts were seeded in 12-well plates and *siSOST*, PBS and a siCtrl encapsulated in LNPs were all administered in triplicate wells as indicated. (**a**) At day 3 and (**b**) day 7 following treatment, *SOST* mRNA expression was determined by qRT-PCR using the comparative ΔΔCT method. The *SOST* mRNA was normalized to housekeeping gene *Hprt*. Bar graphs represent expression of *SOST* mRNA relative to *Hprt* where *SOST* mRNA values following LNP-siRNA-Ctrl treatment are considered 100%. Data are shown as mean ± SD of triplicate wells and are representative of at least three experiments. Bar graphs in (**c**) and (**d**) represent expression of *Tbp* mRNA relative to *Hprt*. *Tbp* mRNA following siCtrl is considered 100% (***$P < 0.001$).

β-*Catenin*, a gene that plays a major role in gene transcription, remained unchanged throughout the treatment suggesting that siRNA-mediated *SOST* knockdown did not affect the signaling pathways involved in cell homeostasis. *Alp* activity is a marker for osteoblast differentiation as proliferating osteoblasts show *Alp* activity that is greatly enhanced during their *in vitro* differentiation and bone formation. To further confirm the osteogenic differentiation of siRNA-mediated *SOST* knockdown in MEFs, cells were treated with OM to induce expression of sclerostin and then were treated with phosphate-buffered saline (PBS), siCtrl and *siSOST* for 1, 2, and 3 weeks in an osteogenic stimulatory medium. After 1 week of treatment, red staining was significantly enhanced in *siSOST*-treated cells compared to siCtrl or PBS, suggesting an increase in ALP activity following *SOST* knockdown (**Figure 5a**,**d**). The ALP staining intensity increased at 2 weeks after treatment and remained significantly higher compared to PBS- and siCtrl-treated cells (**Figure 5b**,**d**). After 3 weeks, ALP staining of *siSOST*-treated cells exhibited a dramatic increase in ALP intensity compared with controls, appearing similar to the OM-treated cells (**Figure 5c**,**d**). These results indicate that siRNA-mediated knockdown of *SOST* gene exhibits an osteogenic effect demonstrated by increased ALP activity and differentiation to osteoblasts.

RNAi-induced prolonged *SOST* silencing without affecting cell viability

Since development of phenotypic effects may require silencing of *SOST* for an extended period, it was important to examine the duration of RNAi-induced silencing after a single treatment. Following *SOST* induction, MEFs were treated with *siSOST* or siCtrl for 3 days. Treatment was stopped after 3 days by replacing the medium, and *SOST* mRNA was measured every 3 days for 2 weeks using real-time qRT-PCR. It was observed that *SOST* transcripts were reduced by 60% 3 days after single treatment with *siSOST*, compared to siCtrl (**Figure 6a**). *SOST* expression reduced progressively demonstrating > 80% knockdown at 12 days post-treatment but began to increase after 2 weeks, but remained significantly reduced compared with siCtrl-treated MEFs. Microscopic monitoring of cells did not reveal overt toxicity over 15 days incubation. Importantly, despite significant downregulation of *SOST*, the *Tbp* housekeeping gene remained unchanged, confirming target specificity of RNA interference (**Figure 6b**). To determine the osteogenic effects on MEFs following a single treatment, mRNA transcripts of three key osteogenic genes *Alp*, *Coll1A1* and *Ocn* was also measured. The data indicate a moderate upregulation of the mRNA of all the tested biochemical markers, which tended to diminish at the

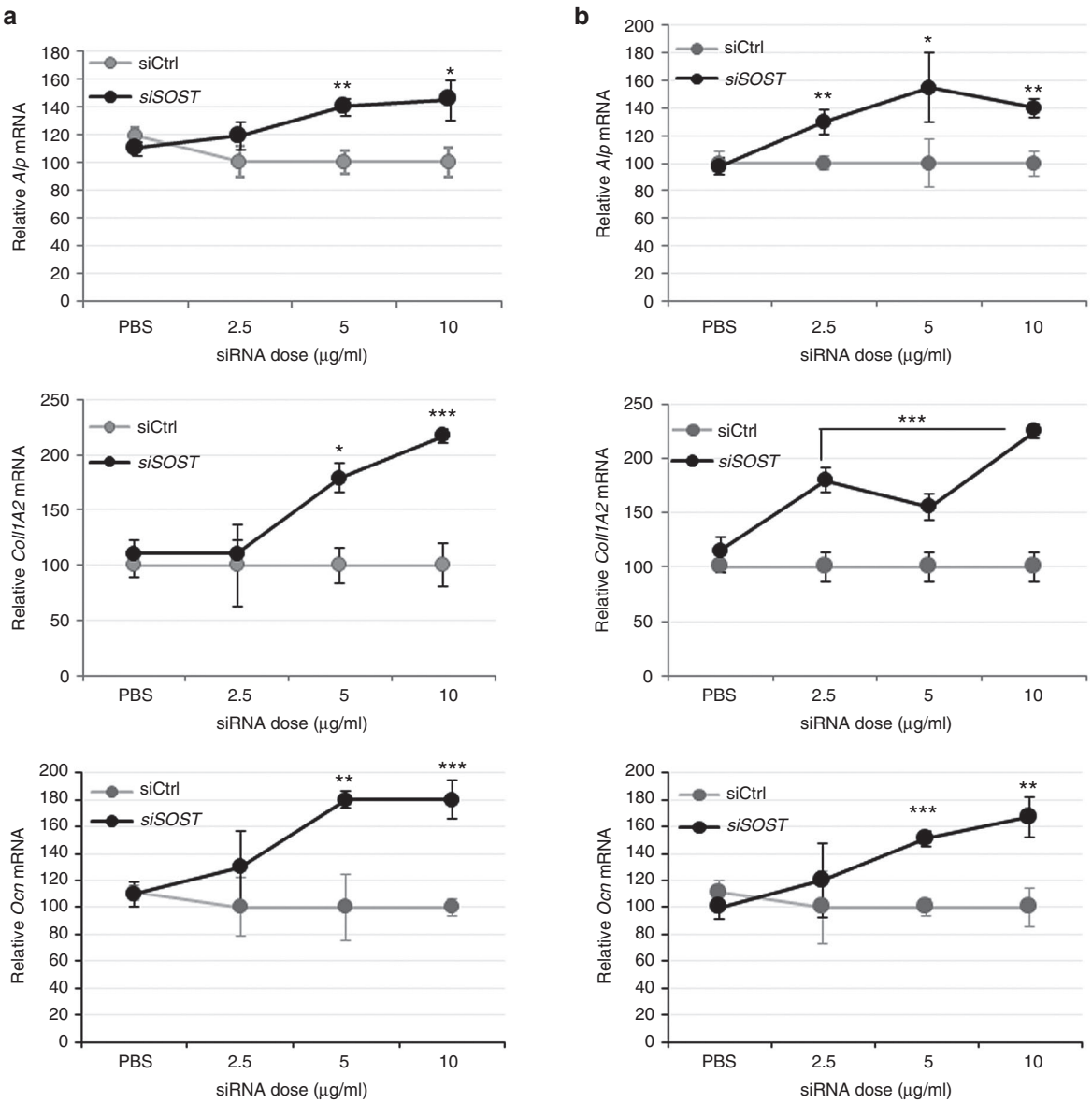

Figure 4 siRNA-mediated *SOST* knockdown increases expression of bone osteogenic markers. mRNA expression of bone osteogenic markers was analyzed using qRT-PCR following *siSOST*, siCtrl, or PBS treatment at indicated doses. Relative expression of target genes was quantified and normalized to the housekeeping gene *Hprt*. The mRNA of *siSOST*-treated samples was compared to siCtrl, which was considered 100%. Graphs depict increases of bone osteogenic markers relative to mRNA expression (**a**) 3 and (**b**) 7 days following treatment with siCtrl that was considered 100%. Data are shown as mean ± SD of triplicate wells and are representative of at least three experiments (*$P < 0.5$; **$P < 0.01$; ***$P < 0.001$).

2 week time point (**Figure 6c**). Taken together, the data suggest that a single dose treatment with *siSOST* delivered with LNPs produced a prolonged silencing effect on the *SOST* gene without compromising cell viability and elicited a moderate but consistent osteogenic effect on MEFs.

siRNA-LNPs exhibit significant uptake by osteocytes *in vivo*

Next, we investigated the uptake of LNP-siRNAs by osteocytes *in vivo*. LNP-siRNA labeled with DiI or PBS were administered intravenously to green fluorescence protein (GFP) expressing mice used as a source of ubiquitous green cells including osteocytes. Forty-eight hours later bone sections were viewed under a confocal microscope. In mice treated with PBS, we could visualize the cellular component of the compact bone, 90% of which consists of osteocytes. Osteocytes were identified based on the expression of GFP in the cytoplasm and nuclei, ellipsoid and stellate shape, regular parallel orientation, and size. The connecting syncytial network, consisting of small cytoplasmic dendritic processes in canaliculi, was also visible at high power (**Figure 7a**). Sections from mice treated with dye-labeled LNP-siRNA (i.v. injection *via* tail vein) demonstrated similar distributions of the red and green staining that almost completely overlapped with the osteocyte-like shapes. Of note, there was unstained area in the center of the red-stained cellular structure corresponding

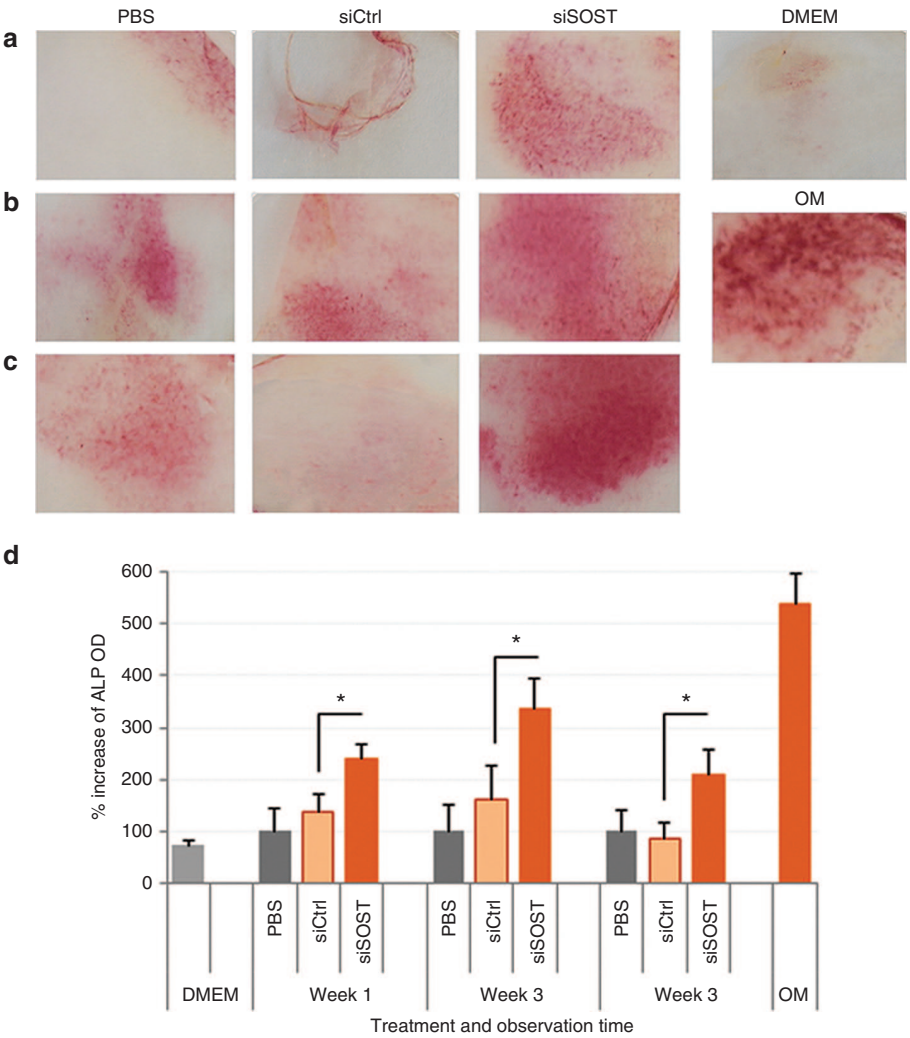

Figure 5 *SOST* knockdown enhances alkaline phosphatase activity. Mouse embryonic fibroblasts (MEFs) were seeded in plates at 60×10^4 cells per cm^2 and incubated with OM. Cells were then treated for 1 week with siRNA-*SOST* or siRNA-Ctrl encapsulated in LNPs, at 10 mg/ml and a plate was treated with PBS. In one plate, cells were incubated in DMEM and in another plate cells were incubated with OM throughout all the observation period. MEFs were subjected to alkaline phosphatase staining (**a**) 1, (**b**) 2, and (**c**) 3 weeks following treatment. ALP activity was assessed based on the red staining intensity using photomicroscopy. A minimum of 3 images were examined for each treatment and time point. Data were analyzed using the OpenLab software. (**d**) Images were quantified as described in Materials and Methods. The bar graphs depict percent increase (mean ± SD, $n = 3$) of ALP activity over time relative to PBS- or siCtrl-treated cells. Data are representative of two different experiments ($^*P < 0.5$).

to the nuclei. These results indicate that a substantial number of osteocytes had taken up significant amounts of dye-labeled LNP-siRNA (**Figure 7b**). The intensity and distribution of the red pattern was quantified relative to green osteocytes, as described. It was concluded that about 50% of the osteocytes had taken up significant amount of LNP-siRNA, as characterized by intracellular accumulation and cytoplasmic distribution of the dye-labeled LNPs.

LNP-siRNA nanosystems induce *SOST* silencing *in vivo* following systemic administration

Since we could achieve knockdown of *SOST in vitro* and confirm delivery of LNP-siRNAs in osteocytes *in vivo*, it was of obvious interest to determine whether these formulations induce *SOST* silencing *in vivo* following systemic administration. In addition, it was important also confirm that *SOST* expression is restricted to osteocytes in compact bone.[3] Total RNA was extracted from mouse bone, heart, kidney, liver, lung, and spleen and mRNA was determined using qRT-PCR. It was observed that *SOST* mRNA was highly expressed in mouse bones (**Supplementary Figure S4**). However, *SOST* mRNA was minimally expressed in kidney, lung, and spleen whereas only traces of *SOST* mRNA were determined in the liver and heart. Since the cellular constituents of compact bone are 90% osteocytes, we can conclude that *SOST* mRNA is expressed almost exclusively in osteocytes. To determine *SOST* silencing following LNP-siRNA administration, mice were injected with LNP containing *siSOST*, non-specific siCtrl or with PBS. Mouse bone and serum were then harvested at 2, 3, and 7 days post-treatment, and circulating sclerostin and *SOST* mRNA were measured using ELISA and qRT-PCR. The data showed that circulating sclerostin was minimally

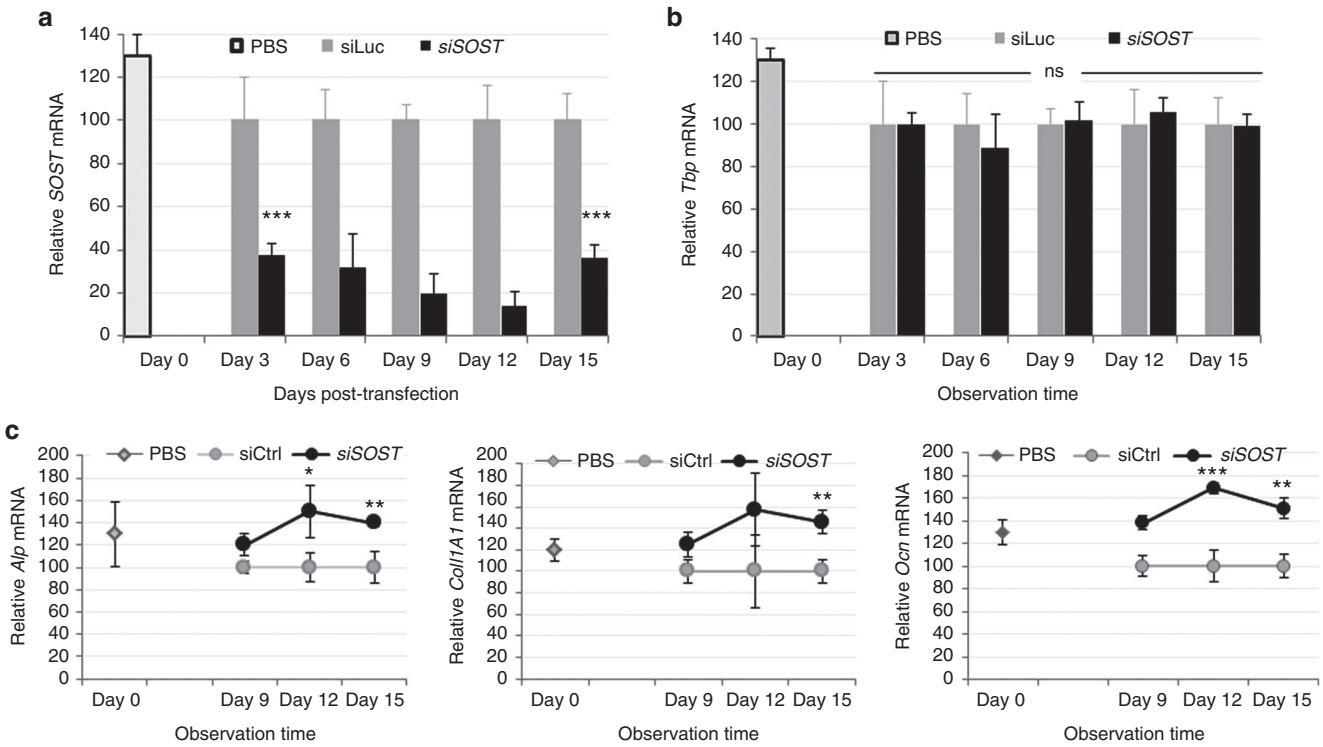

Figure 6 Duration of *SOST* knockdown *in vitro* and its effect on bone osteogenic markers. Sclerostin expression was induced in mouse embryonic fibroblasts followed by treatment with *siSOST* or siCtrl encapsulated in LNPs. After 3 days, siRNA was washed off, the plate was refilled with DMEM and total RNA was extracted every 3 days for over a period of 2 weeks. Total RNA was extracted and mRNA of (**a**) *SOST* (**b**) *Tbp* housekeeping gene and (**c**) bone osteogenic markers was determined using qRT-PCR. Bar graphs represent mRNA expression of *SOST*, *Tbp* and bone osteogenic markers relative to *Hprt* housekeeping gene over time. *SOST* mRNA following siCtrl treatment are considered 100%. Data are shown as mean ± SD of triplicate wells and are representative of at least two experiments (**P* < 0.5; ***P* < 0.01; ****P* < 0.001). ns, not significant.

downregulated at 2 days after treatment (**Figure 8a**), but significant downregulation was observed at 7 days post-treatment ($P = 0.01$, $P < 0.05$). The qRT-PCR analysis revealed significant knockdown of the *SOST* gene at 2 ($P = 0.009$, $P < 0.05$) and 3 days post-treatment ($P = 0.01$, $P < 0.05$) reaching 60% silencing relative to PBS and/or siCtrl ($P = 0.002$, $P < 0.05$) 7 days post-treatment (**Figure 8b**). Noticeably, following treatment with PBS or siCtrl, *SOST* mRNA remained at similar levels, indicating that *siSOST*-mediated silencing was sequence specific. In addition, neither siCtrl nor *siSOST* administration altered the expression of the *Tbp* housekeeping gene, demonstrating that *SOST* knockdown was also gene specific and excluding siRNA-mediated off target effects. In additional experiments, we attempted to optimize the method and improve the quality of RNA extracted from bone. Following a further optimization of RNA extraction from compact bone with further improved RNA Integrity Number above 8 (**Supplementary Figure S5b**), a new *in vivo* investigation was set to confirm *SOST* knockdown *in vivo*. Mice were injected intravenously with *siSOST*, PBS, or two nonspecific control siRNAs targeting luciferase (siLuc) and human androgen receptors (si*ARh*). RNA was extracted 1 week after treatment and *SOST* mRNA expression was measured by qRT-PCR. An aliquot was used to quantitate RNA. The results demonstrate a substantial knockdown of the *SOST* mRNA relative to both negative controls siLuc or siARh, and no difference of *SOST* expression was observed between samples treated with PBS or control siRNA. In addition, none of the siRNA treatments altered the expression of *Tbp* housekeeping gene relative to PBS treatment, confirming the efficacy of LNP-siRNAs to specifically silence the target gene. It is important to note that no treatment-related gross toxic effects were observed, as determined by monitoring weight loss of the mice (**Supplementary Figure S6a,b**). Taken together, these results indicate that the LNP-siRNAs are highly active and very efficient in silencing *SOST* gene expression in compact bone *in vivo*.

Discussion

In this work, we have shown that the *SOST* gene can be induced *in vitro* in primary MEFs, a surrogate stem cell model for bone-marrow-derived stromal stem cells, and have developed an siRNA duplex that effectively silences *SOST* gene expression. Further, we have shown that LNP systems containing *SOST* siRNA can effectively silence *SOST* gene expression both in MEFs *in vitro* and in osteocytes in compact bone *in vivo* following systemic (i.v.) administration. There are three aspects of these results that warrant further discussion. The first area concerns the utility of the MEF cell line for *in vitro* studies and the correlation between the silencing the *SOST* gene *in vitro* with *in vivo* results. The second topic concerns the potential advantages of RNAi therapeutics

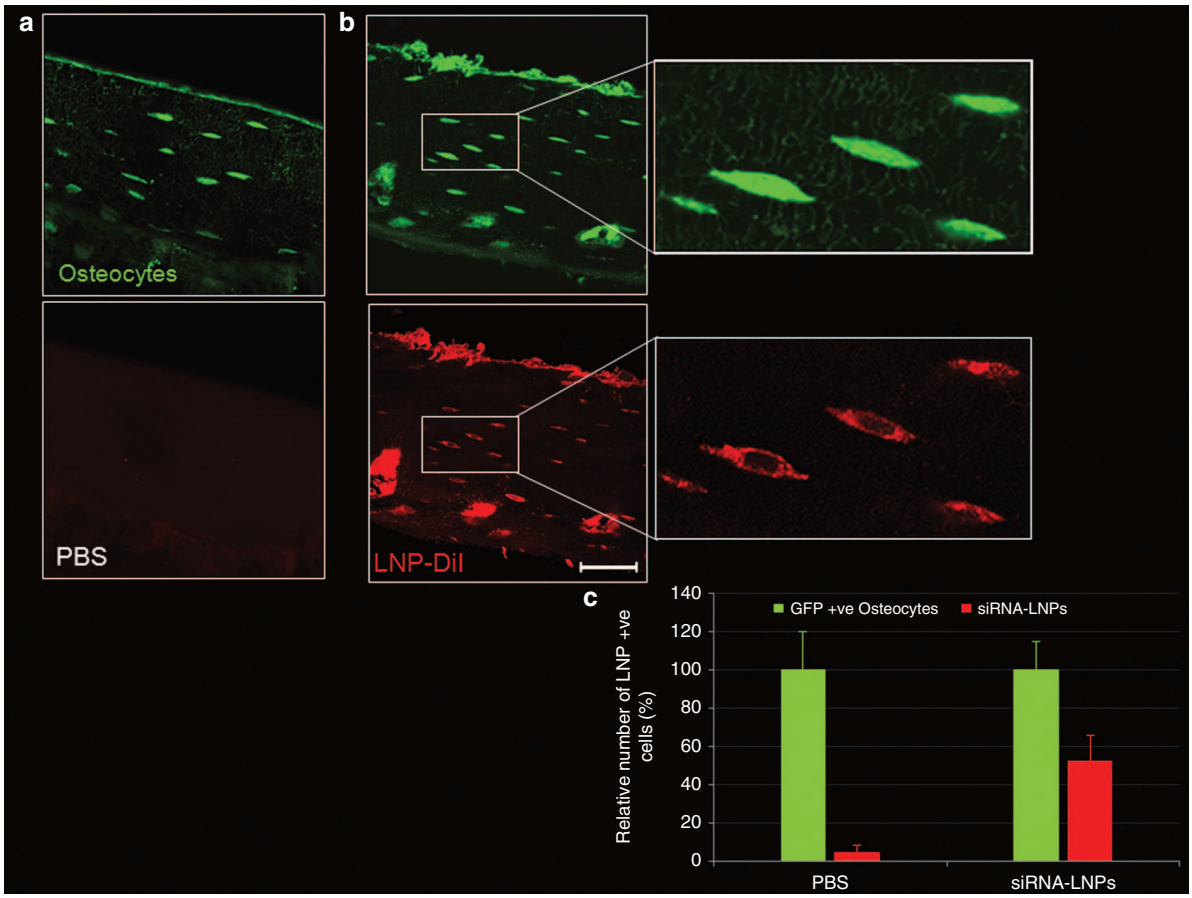

Figure 7 Successful delivery of labeled LNP-siRNA to mouse osteocytes following systemic administration. DiI-labeled LNP-siRNAs (red) were administered intravenously in to GFP mice. Two days following injection, 5 µm bone sections were prepared, processed and analyzed under a confocal microscope. Images depict representative areas of compact bone 48 hours following systemic administration of (**a**) PBS and (**b**) labeled LNP-siRNAs. Ellipsoid shape morphology and parallel orientation suggests that green cell-like structures represent osteocytes whereas the red cell-shaped structures indicate LNP-siRNAs. Images demonstrate a high degree of overlap between osteocytes (green) and LNP-siRNAs (red) indicating the intracellular enrichment with LNP-siRNAs and their delivery to osteocytes. (**c**) The number of osteocytes containing LNP-siRNAs was quantified as described. Graphs demonstrate the percentage of the osteocytes containing LNP-siRNAs vs total number of osteocytes. Approximately 1000 cells were analyzed. Data are representative of two different experiments. Scale bar = 10 µm.

and the limitations of the LNP siRNA system employed here, which was originally designed for silencing genes in hepatocytes following i.v. administration. Finally, we discuss ways in which the therapeutic utility of the LNP siRNA systems could be improved possibly leading to novel treatments for osteoporosis.

The MEF tissue culture system was used as a surrogate for bone-marrow-derived stromal stem cells. MEFs represent a population of stem cells that behave similarly to bone marrow-derived stem cells in *ex vivo* and *in vivo* assays, and have been used to investigate molecular mechanisms of stem cell differentiation to osteoblasts and chondrocytes.[9] Furthermore, it is established that MEFs are capable of entering and completing the program of chondrogenic differentiation *ex vivo*, from undifferentiated progenitor cells to mature chondrocytes, thereby providing a tool that enables the study of a mesenchymal progenitor cell's journey through the chondrogenic pathway.[10]

As visualized by confocal microscopy, the LNP formulations utilized here demonstrated a remarkable ability to deliver siRNA into MEFs, and, following induction of the *SOST* gene (which is usually only expressed in osteocytes), to silence this gene. It may be noted that related LNP siRNA systems have demonstrated abilities to silence genes in erythroid and myeloid progenitors in bone marrow following i.v. administration (Tam Y. *et al.*, unpublished data) suggesting a high potency in nominally "hard to transfect" cell lines. This could be due to the mechanism whereby these LNP siRNA systems are accumulated into cells following association with endogenous ApoE.[11,12] ApoE receptors are expressed at high levels in adult hematopoietic stem cells and in neural stem cells[13,14] In any event, the MEF cell line proved a convenient system to optimize siRNA dimers and demonstrate a functional effect of *SOST* knockdown, as illustrated by the upregulation of bone osteogenic markers such as *Alp* to a level similar to that achieved by incubation in osteotrophic media.

The MEF tissue culture system allowed the development of a potent siRNA duplex for silencing the *SOST* gene and showed that LNP systems containing this duplex could result in gene silencing, leading to *in vivo* studies to see whether

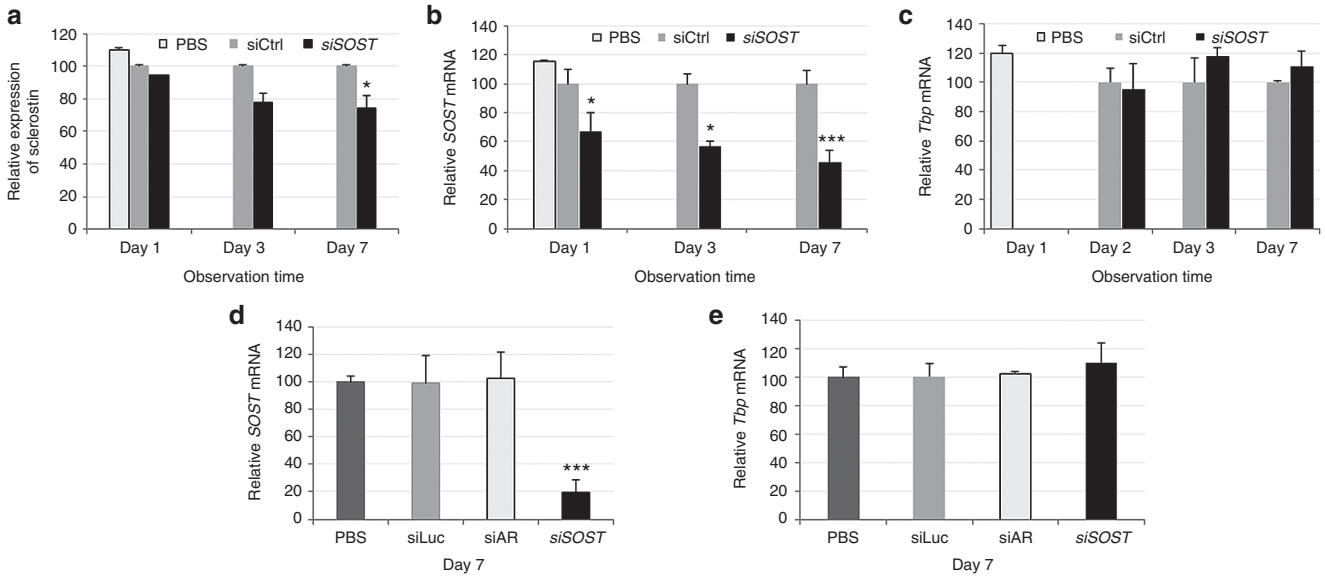

Figure 8 LNP-siRNA mediated silencing of *SOST in vivo* is specific, time dependent and very effective. (**a**) LNP-siRNA targeting *SOST*, LNP-siCtrl or PBS, were administered intravenously in to C57Bl6 mice. Blood was collected and serum sclerostin was determined using the enzyme-linked immunosorbent assay Bar graphs depict sclerostin expression overtime in mice administered with *siSOST* relative to siCtrl treatment. Sclerostin levels following siCtrl treatment were considered 100%. $P < 0.05$. Following *in vivo* administration with *siSOST*, siCtrl or PBS, femurs and tibae were dissected, total RNA was extracted and *SOST* and *Tbp* mRNA was determined at time points indicated. Bar graphs represent expression of (**b**) *SOST* and (**c**) *Tbp* mRNA overtime relative to *Hprt*. *SOST* mRNA values following siCtrl treatment are considered 100%. Data are representative of 3 different experiments. (**c**) After *in vivo* administration of *siSOST* and siCtrl (s) as described, high quality RNA were obtained and *SOST* and *Tbp* mRNAs were measured. Bar graphs represent expression of (**d**) *SOST* and (**e**) *Tbp* mRNA relative to *Hprt* seven days after administration of *siSOST*. mRNA expression of *SOST* following siCtrl treatment are considered 100%. $*P < 0.5$ $***P < 0.001$.

similar effects could be observed in osteocytes in compact bone. In this regard, a primary challenge for the development of siRNA therapeutics is the ability to deliver siRNA molecules to target organs or cells *in vivo*. RNAi therapeutics were originally limited to topical applications[15] but dramatic improvements in LNP systems for hepatocyte gene silencing have enabled liver targets to be exploited.[16,17] However, LNP systems to target other tissues are less developed.[18] LNP containing permanently charged cationic lipids have been shown to silence target genes on bone-forming surfaces following systemic administration,[19,20] but permanently charged cationic lipids can be highly toxic.[21,22] The studies presented here show effective delivery of LNP-siRNA to osteocytes following i.v. administration as visualized by confocal microscopy, demonstrating the presence of LNP-siRNA in at least 50% of osteocytes. This delivery was accompanied by significant knockdown of the *SOST* gene in these osteocytes and consequent downregulation of serum sclerostin 1 week after systemic administration of siRNA. It is of interest that levels of *Alp* did not change during the week after siRNA administration, and other markers were only slightly downregulated. A recent study demonstrated that for menopausal women with low bone mineral density, the increase in bone-formation markers following administration of anti-sclerostin antibody were transitory and were only detected 1 week after the initial dose, and were largest 1 month after. However treatment with the antibody was associated with increased bone mineral density and bone formation. It is likely that wild-type mice are not the ideal model to study the effect of siRNA-mediated knockdown of *SOST*, particularly with regard to effects on osteogenic markers.

With regard to the potential advantages of RNAi-based therapies for treatment of disorders such as osteoporosis, inhibition of sclerostin using monoclonal antibodies has been shown to restore bone loss induced by estrogen deficiency, and increase bone mass and strength in animal models or postmenopausal osteoporosis in humans.[10,23,24] Therefore, inhibition of the Wnt/β-catenin signaling pathway represents a promising therapeutic target for osteoporosis treatment.[25] However, the sclerostin antibody can cause an immune response leading to rapid clearance and reduced potency for repeat administrations.[26] RNAi-based therapies that silence the *SOST* gene in osteocytes could provide a more effective approach that may not be subject to such limitations. It has been noted that transthyretin (TTR) gene silencing in hepatocytes can persist for up to 60 days following i.v. administration of LNP TTR siRNA in humans.[16] In addition, recent work has shown that incorporation of hydrophobic corticosteroid pro-drugs in LNP successfully abrogates immune responses to LNP oligonucleotide formulations (S. Chen, unpublished data). A final point is that, regardless of potential clinical applications, the studies presented here show that LNP-siRNA systems are potentially a powerful tool to study loss of function effects for novel gene targets in animal disease models of bone disorders.

While LNP siRNA systems to silence genes such as *SOST* may have therapeutic potential, it is important to note the limitations of the LNP siRNA system employed in this work, which contains the ionizable cationic lipid DLin-MC3-DMA, the neutral lipids DSPC and cholesterol together with a PEG-DMG coating lipid. This system has demonstrated remarkable efficacy for gene silencing in hepatocytes following i.v.

administration in mice and nonhuman primates[27] and has recently been shown to be highly effective for treating TTR-induced amyloidosis in advanced clinical trials.[16,28] However, when applied to silencing genes in extra-hepatic tissues such as bone, these LNP systems are much less potent. In mice, 50% gene silencing of target genes in hepatocytes can be achieved at dose levels as low as 0.005 mg siRNA/kg body weight.[27] In contrast, the doses required to achieve the *SOST* gene silencing observed in this work are 15 mg siRNA/kg body weight, more than a thousand times higher. It is a measure of the relative lack of toxicity of the LNP siRNA systems that such doses are not overtly toxic, however in other work, we have noted toxic effects for repeat doses in the range of 10 mg siRNA/kg body weight (G. Basha, unpublished data). These toxicities arise primarily from the LNP carrier which can be hepatotoxic at high-dose levels. While little toxicity was observed here, doses of 10 mg siRNA or higher are approaching the maximum tolerated dose and cannot be considered as having potential therapeutic utility, an increase in potency in the range of 100 is required.

There are a number of ways in which such large improvements in potency may be achieved. The first concerns circulation lifetime; as noted elsewhere,[29,30] LNP systems containing the coating lipid PEG-DMG (which has C_{14} acyl chains) exhibit short (< 1 hour) circulation lifetimes which limits its distribution to extra-hepatic tissues. Longer circulation lifetimes and enhanced distribution to fenestrated tissues such as bone marrow can be achieved by incorporating PEG-lipids with longer acyl chains, such as PEG-DSG (containing C_{18} acyl chains) which does not dissociate from the LNP as rapidly as PEG-DMG.[30] LNP size is another important variable; it has been noted that smaller nanoparticulate systems exhibit enhanced penetration into tumor tissue.[31,32] By analogy, it would be expected that smaller LNP systems, which can be readily achieved by increasing PEG content[29,33] will improve delivery to the microvasculature of compact bone. An alternative approach concerns the observation that as much as 70% of endocytosed LNP systems are recycled to the extracellular medium, the presence of agents that reduce or delay such recycling can lead to substantial improvements in gene silencing potency.[34]

In conclusion, the studies presented here using the MEF primary cell system establish a model *in vitro* system to study the effects arising from silencing specific genes, such as the *SOST* gene, on osteogenesis. Further, it is shown that non-optimized LNP formulations of siRNA can access osteocytes in hard bone following i.v. administration, resulting in *SOST* gene silencing. This work sets the stage for the development of next-generation LNP siRNA systems that may provide effective strategies for treatment of osteoporosis and other bone diseases.

Materials and methods

Cell culture. Primary mouse embryonic fibroblasts (MEFs) were harvested, according to standard protocols.[35] Briefly, uteri were harvested at the embryonic stage at 13.5 days post-coitus and further processed to isolate the embryos and MEFs. Heads and viscera were removed and the remaining embryos were washed in PBS, transferred to 35 mm petridishes, minced with pair of scissors and digested with 0.25% trypsin/EDTA 1 mmol/l (Sigma-Aldrich, St. Louis, MO) for 10 minutes at 37 °C. Following digestion, about 3 ml Dulbecco's modified Eagle medium (DMEM), supplemented with 10% fetal bovine serum (FBS), 1% L-glutamine, and 1% penicillin and streptomycin (P/S), was added and the tissue pipetted up and down to get a single cell suspension. MEFs were maintained in T–75 flasks in DMEM, supplemented with 10% FBS, 1% L-glutamine, 1% NEAA, 1% sodium pyruvate, and 1% P/S until 80–85% confluent and were then passaged at a 1:2 ratio. In this study, we used MEFs at passage 3.

SOST induction, siRNA transfection, and sequence identification. MEFs were seeded in 12-well plates at a density of 6×10^4 cells/cm^2 and incubated with DMEM, 10% FBS, and 1% P/S. At 80% confluence, cells were incubated with MesenCult Osteogenic Stimulatory Kit (STEMCELL Technologies, Vancouver, Canada) or Osteogenic Medium (OM). The MesenCult Osteogenic Stimulatory Kit (Mouse) is specifically formulated for the *in vitro* differentiation of mouse mesenchymal stem and progenitor cells from compact bone, bone marrow, and MEFs into osteoblasts. This kit induces strong osteogenesis in mouse MSCs and MEFs. Media were changed every second day for 15 days. Every 3 days, cells from triplicate wells were lysed using 350 µl lysis buffer (Invitrogen, Carlsbad, CA) and stored at –80 °C. At the end of the experiment, cell lysates were thawed, mixed with equal amounts of 70% ethanol, and RNA was extracted according to the manufacturer's directions (PureLink RNA extraction Kit, Life Technologies). Extricated total RNA was used to determine mRNA expression of *SOST*, alkaline phosphatase (*Alp*), an early bone osteogenic marker, *Sp7* (master regulator of osteoblast differentiation), *RunX2* (a key transcription factor associated with osteoblast differentiation), and bone sialoprotein (*Bsp*), a component of mineralized tissues. The mRNA expression levels of *SOST* or bone osteogenic genes were quantified by real-time polymerase chain reaction (qRT-PCR). PureLink RNA Mini Kits (Life Technologies) were used to extract total RNA from cultured cells using the commercial protocol. RNA was reverse transcribed to complementary DNA (cDNA) from 1 µg of total RNA from each sample, using a High Capacity cDNA Reverse Transcription kit (Applied Biosystems, Foster City, CA). Real-time PCR was performed on a StepONE Plus Real Time PCR system (Applied Biosystems) using TaqMan Fast Advanced Master Mix (Applied Biosystems), which include forward and reverse primers and the fluorescein amidite (FAM)-labeled probe for the target gene respectively purchased from Integrated DNA Technologies, Iowa. In addition, protein was extracted from designated plates and determined as previously described,[28] followed by quantification using NIH ImageJ-win32 software in order to measure sclerostin expression at 7 and 14 days following incubation in OM. Another set of plates containing MEFs incubated in DMEM or OM were used to measure alkaline phosphatase activity following treatment with DMEM or OM that was quantified as described below. To test the efficacy of gene-specific siRNA on MEFs *in vitro*, a set of three predesigned duplexes (TriFECTa, Integrated DNA Technologies) were used, namely A, B, and C, including three

additional duplexes, D, E, and F, all from the RefSeq database in GenBank (**Supplementary Table S1**). To optimize the experimental setting of RNAi for our target gene *SOST*, three controls were used: a fluorescent dye-labeled duplex (Tye 3 DS transfection control), a "universal" negative control duplex (NC1) that targets a site that is absent from human, mouse and rat genomes, and a positive control duplex (*Hprt*-S1 DS-positive control) that targets a site in the hypoxanthine phosphoribosyntransferase (*Hprt*) 1 gene common between human, mouse, and rat. MEFs were seeded in 24-well plates and forward transfection was performed in triplicate according to the manufacturer's directions, by mixing the RNAiMax (Invitrogen) transfection reagent with siRNA to obtain a final concentration of 3,10, and 30 nmol/l, including positive and negative controls. Transfection progressed for 2 hours before the first medium renewal. After 24 and 48 hours in culture, cells were lysed with 350 µl lysis buffer (Life Technologies) and stored at –80 °C. Transfection efficiency was assessed following intracellular visualization of Tye 563-labelled siRNA using a Zeiss Axiovert 200 microscope with a QImaging Retiga EX mono 12-bit camera. Fluorescence and phase-contrast images were overlaid to visualize the intracellular siRNA using confocal microscopy.

Preparation of lipid nanoparticles (LNPs) and siRNA encapsulation. LNPs were prepared by mixing one volume of the following lipid composition dilinoleylmethyl-4-dimethylaminobutyrate (DLin-MC3-DMA), distearoylphosphatidylcholine (DSPC), cholesterol, and polyethylene glycol-dimyristol glycerol (PEG-DMG) at 50:10:38.5:1.5 mole ratio) dissolved in ethanol and three volumes of siRNA (1:10 w/w siRNA to lipid) suspended in acetate buffer. The cationic lipid was synthesized by Biofine International (Vancouver, BC). A detailed description of the cationic lipid and its activities has been described previously.[27] Formulation was performed in a microfluidic mixer, provided by Precision Nanosystems (Vancouver, BC), by pumping both solutions through the micromixer at a combined flow rate of 4 ml/minute (1 ml/minute for ethanol and 3 ml/minute for aqueous buffer). The resultant mixture was dialyzed against phosphate-buffered saline (PBS), pH 7.4 for 16 hours to remove ethanol, and then filtered. A detailed description of the method has been described previously.[29] To prepare fluorescently labelled LNPs, 0.2 mol% 1,1'-Dioctadecyl-3,3,3',3'-Tetramethylindodicarbocyanine-5,5'-disulfonic acid (DiI-C_{18}) from Invitrogen, was added to the lipid mix. Dynamic light scattering was used to determine LNP size (number weighting) using the Malvern Zetasizer NanoZS (Worcestershire, UK). Size measurements were performed in PBS (pH 7.4). Encapsulation was measured using the Quant-iT Ribogreen RNA assay (Life Technologies, Burlington, ON). Particles were incubated at 37 °C in the presence or absence of 1% Triton X-100 (Sigma-Aldrich, St. Louis, MO) for 10 minutes. Following incubation, Quant-iT Ribogreen RNA reagent was added and fluorescence intensity measured (Ex/Em 480/520 nm). Triton X-100 treatment measurements represented total siRNA while non-Triton X-100 treatments represented un-encapsulated siRNA.

Intracellular delivery of siRNA, knockdown efficiency in vitro, and quantitative real-time PCR (qRT-PCR). Prior to testing knockdown efficiency, it was important to assess the siRNA delivery in primary MEFs following encapsulation in LNPs. 80% confluent MEFs were seeded in 35-mm glass bottom culture dishes (MatTek Corporation, MA) at appropriate concentrations and LNPs containing siRNA labeled with Quasar 570 Ex/Em 548/566 nm, were added to the cells at a concentration of 5 µg/ml. In another separate, parallel experiment, LNPs labeled with DiI (DiI C18 Ex/Em 549/565 nm, Invitrogen) containing siRNA were also incubated with MEFs at the same siRNA concentration. The siRNA was encapsulated in LNPs containing DLin-MC3-DMA and cellular uptake of siRNA and LNPs was monitored for 15, 30, 60, and 120 minutes by measuring the accumulation and the intensity of the fluorescence of DiI and Quasar 570 in MEFs. The incubation was stopped by removing the media containing the LNP-siRNAs and replenishing the cells with FluoroBrite DMEM (Life Technologies) without Phenol red as a pH indicator. Next, live cell imaging was conducted using a Leica TCS SP8 laser scanning confocal microscope (Leica, Germany) and all images were processed and recorded using LAS AF 3 software. The DiI and Quasar 570 fluorescent probes were excited with the 561 nm laser and the intracellular presence of LNP-siRNAs was examined using NIH ImageJ-win32 and Photoshop 9.0 CS2. Fluorescence and phase-contrast images were overlaid to determine presence and intensity of fluorescence. A minimum of three images were examined for each time point. Data analysis and quantification of intracellular delivery of LNP-siRNA was performed using the NIH ImageJ-win32 as described below.

To better investigate the intracellular delivery of LNP-siRNA a pulse-chase experiment was undertaken. MEFs were grown in 24-well plates, treated with 2 µg/ml siRNA-Alexa647 (far red) in a free form or encapsulated in LNPs DiO (green) from Invitrogen, including PBS control, and maintained at 37 °C. Incubation was stopped after 2 hours by washing off the media and refilling the plate with fresh media. Cells were harvested after 2, 4, 6, 8, 24, and 48 hours. Following treatment, MEFs were trypsinized (0.25% Trypsin), transferred into microcentrifuge tubes, spun at 12,000 × rpm for 4 minutes and after three washes they were resuspended in 300 µl FACS staining buffer. Samples were acquired using an LSRII flow cytometer to assess the presence of LNP (DiO) and siRNA-Alexa647 intracellularly. The Alexa647 fluorophore was excited using the HeNe 633 laser line and detected at the Alexa647 (FL 5) channel whereas the DiO was excited by the Argon laser and detected at FL1 channel. Data were acquired using FACSDiva software and analyzed by FlowJo software. Measurements were collected for 5000 events. Fluorescence intensity was normalized against the PBS controls and was expressed as percent increase of mean fluorescence intensity.

To investigate the siRNA-mediated knockdown, MEFs were seeded in 12-well plates as described. The sequence of the mouse *SOST* gene (GenBank accession no. NM_024449(1) was extracted from the NCBI Entrez nucleotide database. The *SOST*-siRNA was composed of two complementary RNA strands: sense strand (*SOST*-S) 5′-mGmCrAmGrUmGrUrUrAr ArUmArUmCrGmCrUmUrUrGrUrGrAmAG-3′ and antisense strand (*SOST*-AS): 5′-rCrUmUrCrArCrArAmArGmCrGmArUr ArUrUrArArCrArCmUrGmCmCmU-3′. The two strands of

the *SOST*-siRNA are modified oligoribonucleotides that include multiple 2′-OMe modifications (denoted by the letter "m") introduced into the siRNA to improve nuclease stability and also to reduce the risk of pure RNA triggering an innate immune response in mammalian cells.[36] In addition, the 2' O methyl bases represent a modification of RNA that increase stability of interactions making them resistant to attack by single stranded ribonucleases and less susceptible to DNases, thereby increasing stability and binding affinity to the target. MEFs were incubated in OM to induce expression of sclerostin and after 7 days in culture, the selected siRNA duplexes targeting *SOST* (**Supplementary Table S1**), or negative control siRNA (siLuciferase S: cuuAcGcuGAGuAcuucGAdTsdT AS: UCGAAGuACUcAGCGuAAGdTsdT) encapsulated in DLinMC3-DMA LNPs, were added at 2.5, 5, and 10 µg/ml final concentration and incubated as required at low O_2 conditions (37 °C and 5% CO_2 and 5% O_2). The control siRNA against luciferase contains phosphorothioate linkages (indicated as the letter "s") between the 3′-deoxythymidine (dT) overhangs and the control includes multiple 2′-OMe modifications (indicated by lower-case letters). Each siRNA dose was administered in triplicate. One triplicate of wells was treated with PBS and served as a negative control. The media was changed every 3 days while the siRNA was maintained at the required concentrations throughout the entire incubation time. At days 3 and 7 of treatment, or every 3 days for 2 weeks when indicated, cells were lysed with 350 µl of lysis buffer and stored at −80 °C freezer. The mRNA expression levels of *SOST* or bone osteogenic genes were quantified by qRT-PCR and RNA was reverse transcribed to complementary DNA (cDNA) from 1 µg of total RNA. Real-time PCR was performed on a StepONE Plus Real Time PCR system which include forward and reverse primers and the FAM-labeled probe for the target gene respectively (**Supplementary Table S2**). Relative expression between samples was quantified using the comparative $\Delta\Delta C_T$ algorithm and the amount of mRNA of each gene was normalized to the housekeeping gene mouse Hypoxanthine Phosphoribosyltransferase (*Hprt*). When indicated, the mRNA of siRNA treated samples was compared to siRNA control (siCtrl) treated sample, which was considered as 100% being equivalent to no efficacy.

Alkaline phosphatase staining. MEFs were plated in 35 mm Petri dishes at 60×10^4 cells per cm^2 in DMEM supplemented with all additives and incubated at 37 °C and 5% CO_2, low O_2 as described, to reach full confluence. At day 3, DMEM was removed and cells were incubated in OM to induce sclerostin. One week following incubation, OM replaced with DMEM and cells were treated for 1 week with siRNA targeting *SOST*, with an unspecific siCtrl at doses of 10 mg/ml, or treated with PBS. One plate was treated with PBS and cells were incubated with DMEM for the entire incubation time of 3 weeks, and in another plate cells were incubated with OM throughout all the observation period. Media was changed every 3 days and ALP activity was measured in groups of plates that were treated with PBS, siCtrl, and *siSOST* at 1, 2, and 3 weeks after treatment. Media was removed, plates were washed with PBS and fixed with 5% formaldehyde at room temperature for 5 minutes. Next, the fixative was rinsed thoroughly and the cells were incubated with the ALP staining solution containing Napthol AS-MX phosphate (Sigma-Aldrich) 0.1 mg/ml and Fast red violet LB salt (Sigma-Aldrich) 0.65 mg/ml for 1 hour, protected from light. Alkaline-Dye mixture was then discarded, the cells were rinsed thoroughly with deionized water for 2 minutes and plates were allowed to dry. Cells were viewed under a Zeiss Axiovert 200 microscope. A minimum of three images were examined for each treatment and time point. The data were analyzed using the OpenLab software. Quantification of all alkaline phosphatase staining was done in at least three acquired images and in multiple areas of each image using the NIH ImageJ win-32 software. For this, RGB color-type images were analyzed using the Color Deconvolution plugin 1.7 and for each region of interest (ROI) the FastRed FastBlue option was selected to quantify the staining measured following selection of the required setting.[37]

Assessment of LNP-siRNA delivery in vivo using laser scanning confocal microscopy. Eight-week-old C57Bl/6-GFP female mice from our breeding colony, housed at Animal Research Unit, University of British Columbia were used. All animal experiments in this study were performed according to approved protocols and in compliance with the guidelines in accordance with the requirements of Canadian Council and UBC Committee on Animal Care. siRNA-LNP-DiI labeled ($DiIC_{18}$, Invitrogen) formulations were administered intravenously through tail-vein injection at a dose of 15 mg/kg. Two days following injection, mice were euthanized, bones were dissected, the marrow was flushed and bones were fixed in 10% PBS. Bones were then decalcified in a 0.5M ethylenediaminetetraacetic acid (EDTA) solution containing 0.2% glycerol and 0.6% sodium hydroxide, pH 7.1 for several days then processed overnight in 2 changes of 95% ethanol, 4 changes of 100% ethanol, 3 changes of xylene, and 3 changes of wax) for a total of 15.5 hours. Bones were then embedded in wax and sectioned at 5 µm thickness using Leica microtome. Once dry, bone tissues were placed on slides and transferred to an oven at 60° for about 2 hours to dewax and then covered with a coverslip. All Z-stack images were acquired using a Leica TCS SP8 laser scanning confocal microscope (Leica, Germany) and images were recorded and analyzed using LAS AF 3 software. The GFP was excited with a 488 nm argon laser and DiI was excited with a 561 nm laser. Quantification of images was done by calculating the corrected total cell fluorescence (CTCF) in the area selected. CTCF = Integrated density – (area of selected cell × mean fluorescence of background readings). Integrated intensity (area, minimum and maximal gray value, and integrated density) is generated by NIH ImageJ-win32 after selecting the cell of interest.[38] Approximately 1,000 cells were analyzed.

RNA isolation, siRNA knockdown in vivo, and sclerostin measurement. C57Bl/6 female mice (Charles-River) were used to extract total RNA and measure *SOST* mRNA in bones, heart, kidney, liver, lung, and spleen. Three mice per measurement were used. Mouse heart, kidney, liver, lung, and spleen were harvested and 10 mg of tissue was transferred into a FastPrep tube followed by flash-freezing performed by dipping in liquid nitrogen. After adding a ceramic sphere and

350 lysis buffer (PureLink), the tube was placed in a FastPrep tissue and cell homogenizer (MP Biomedicals, Solon, OH). The tissue was then homogenized at 4 m/s for 20 seconds. The lysate was transferred into an RNase–free 1.5 ml Eppendorf tube and RNA purification was performed according to manufacturer's directions. RNA extraction from bones was performed by the liquid nitrogen and mortar and pestle method (see below). For the *SOST* knockdown, C57Bl6 mice were injected intravenously with LNP-siRNA targeting *SOST* or nonspecific siCtrl (luciferase or androgen receptor). Three mice per time point were used at 15 mg/kg. Mice were euthanized 2, 3, and 7 days after LNP-siRNA administration bones were harvested and processed to extract RNA. Initially a two-step method was used consisting of dissecting femurs and tibias, flushing the marrow, snap freezing them in liquid nitrogen, and storing them in –80 °C until further use. In a second attempt, a one-step method was used whereby following dissection, the marrow was flushed out and bones were immediately processed for RNA isolation. Bones were crushed using mortar and pestle while immersed in liquid nitrogen. Once pulverized, the content was poured into 50 ml Falcon tubes. Next, ice-cold TRIzol reagent (Life Technologies) was added to the mix and the content was resuspended thoroughly followed by addition of chloroform. 100% isopropanol was added to the aqueous phase followed by centrifugation to precipitate the RNA. The final RNA was eluted using the PureLink RNA Mini Kit protocol as described. RNA quality and quantity was obtained using Agilent 2100 Bioanalyzer Instrument and RNA Integration Number (RIN) values above 7 were considered suitable for qRT-PCR analysis. Blood was collected from the lateral saphenous vein of mice treated with LNP-siRNA targeting *SOST* gene, or LNP-siRNA unspecific controls and circulating sclerostin was measured. The serum was obtained by spinning the blood at 3,000 rpm, for 10 minutes at 15 °C. Serum was then aliquoted and stored at –80 °C for further assessment. Quantitative determination of sclerostin in mouse serum following siRNA-LNP treatment was achieved using the mouse sclerostin ELISA Assay (ALPCO, Salem, NH) which is a sandwich type immunoassay that employs a 96-well microplate precoated with a polyclonal antibody specific for mouse sclerostin. The assay sample and buffer were incubated together with the HRP conjugate on the precoated plate followed by incubation with a substrate for HRP enzyme. The product of the enzyme-substrate reaction produced a color that was measured spectrophotometrically at 450 nm in a microplate reader (OpsysMR DYNEX Technologies). Recombinant mouse sclerostin was used for the generation of a standard curve (standard curve range 1,200–37.5 pg/ml). None of the measured values of sclerostin in serum samples was below the limit of detection of the assay (LLOQ = 37 pg/ml).

Statistical analysis. Experimental values are presented as mean ± SD and expressed in percent from 100% baseline. The "n" value represents the number of experiments conducted for analysis. Statistical analyses were performed using a two-tailed Student's *t*-test, two tails, where always two groups were compared at each time point indicated (*i.e.*, siCtrl vs. *siSOST* or PBS vs. osteogenic medium treated samples). The type (paired or two-sample equal variance-homoscedastic), was determined based on the variation of the standard deviation of two populations. $P < 0.05$ was accepted as statistically significant ($^{*}P < 0.05$; $^{**}P < 0.01$; $^{***}P < 0.001$).

Acknowledgments The authors would like to acknowledge support from the Canadian Institutes for Health Research (CIHR) under UOP grant 122069.

Supplementary material

Figure S1. Identification of the siRNA sequence targeting *SOST*.
Figure S2. The 2'OMe modifications do not affect the siRNA-mediated *SOST* knockdown.
Figure S3. Modulation of expression of bone osteogenic markers following *SOST* siRNA is dose and time dependent
Figure S4. *SOST* expression is restricted to osteocytes.
Figure S5. Improved method of RNA extraction from compact bone yielded more and better quality of total RNA.
Figure S6. Animals treated with LNP-siRNAs did not show weight loss.
Table S1. siRNA sequences screened in the study.
Table S2. Primer sequences of the genes determined in the study.

1. Klibanski, A, Adams-Campbell, L, Bassford, T, Blair, SN, Boden, SD, Dickersin, K *et al.* (2001). Osteoporosis: prevention, diagnosis and therapy. *JAMA* **285**: 785–795.
2. Moon, RT, Bowerman, B, Boutros, M and Perrimon, N (2002). The promise and perils of Wnt signaling through beta-catenin. *Science* **296**: 1644–1646.
3. Poole, KE, van Bezooijen, RL, Loveridge, N, Hamersma, H, Papapoulos, SE, Löwik, CW *et al.* (2005). Sclerostin is a delayed secreted product of osteocytes that inhibits bone formation. *FASEB J* **19**: 1842–1844.
4. Brunkow, ME, Gardner, JC, Van Ness, J, Paeper, BW, Kovacevich, BR, Proll, S *et al.* (2001). Bone dysplasia sclerosteosis results from loss of the *SOST* gene product, a novel cystine knot-containing protein. *Am J Hum Genet* **68**: 577–589.
5. Winkler, DG, Sutherland, MK, Geoghegan, JC, Yu, C, Hayes, T, Skonier, JE *et al.* (2003). Osteocyte control of bone formation via sclerostin, a novel BMP antagonist. *EMBO J* **22**: 6267–6276.
6. Hamersma, H, Gardner, J and Beighton, P (2003). The natural history of sclerosteosis. *Clin Genet* **63**: 192–197.
7. Vanhoenacker, FM, Balemans, W, Tan, GJ, Dikkers, FG, De Schepper, AM, Mathysen, DG *et al.* (2003). Van Buchem disease: lifetime evolution of radioclinical features. *Skeletal Radiol* **32**: 708–718.
8. McClung, MR, Grauer, A, Boonen, S, Bolognese, MA, Brown, JP, Diez-Perez, A *et al.* (2014). Romosozumab in postmenopausal women with low bone mineral density. *N Engl J Med* **370**: 412–420.
9. Saeed, H, Taipaleenmäki, H, Aldahmash, AM, Abdallah, BM and Kassem, M (2012). Mouse embryonic fibroblasts (MEF) exhibit a similar but not identical phenotype to bone marrow stromal stem cells (BMSC). *Stem Cell Rev* **8**: 318–328.
10. Lengner, CJ, Lepper, C, van Wijnen, AJ, Stein, JL, Stein, GS and Lian, JB (2004). Primary mouse embryonic fibroblasts: a model of mesenchymal cartilage formation. *J Cell Physiol* **200**: 327–333.
11. Yan, X, Kuipers, F, Havekes, LM, Havinga, R, Dontje, B, Poelstra, K *et al.* (2005). The role of apolipoprotein E in the elimination of liposomes from blood by hepatocytes in the mouse. *Biochem Biophys Res Commun* **328**: 57–62.
12. Akinc, A, Querbes, W, De, S, Qin, J, Frank-Kamenetsky, M, Jayaprakash, KN *et al.* (2010). Targeted delivery of RNAi therapeutics with endogenous and exogenous ligand-based mechanisms. *Mol Ther* **18**: 1357–1364.
13. Murphy, AJ, Akhtari, M, Tolani, S, Pagler, T, Bijl, N, Kuo, CL *et al.* (2011). ApoE regulates hematopoietic stem cell proliferation, monocytosis, and monocyte accumulation in atherosclerotic lesions in mice. *J Clin Invest* **121**: 4138–4149.
14. Gan, HT, Tham, M, Hariharan, S, Ramasamy, S, Yu, YH and Ahmed, S (2011). Identification of ApoE as an autocrine/paracrine factor that stimulates neural stem cell survival via MAPK/ERK signaling pathway. *J Neurochem* **117**: 565–578.
15. Haussecker, D (2012). The business of RNAi therapeutics in 2012. *Mol Ther Nucleic Acids* **1**: e8.
16. Coelho, T, Adams, D, Silva, A, Lozeron, P, Hawkins, PN, Mant, T *et al.* (2013). Safety and efficacy of RNAi therapy for transthyretin amyloidosis. *N Engl J Med* **369**: 819–829.

17. Fitzgerald, K, Frank-Kamenetsky, M, Shulga-Morskaya, S, Liebow, A, Bettencourt, BR, Sutherland, JE *et al.* (2014). Effect of an RNA interference drug on the synthesis of proprotein convertase subtilisin/kexin type 9 (PCSK9) and the concentration of serum LDL cholesterol in healthy volunteers: a randomised, single-blind, placebo-controlled, phase 1 trial. *Lancet* **383**: 60–68.
18. Wang, Y and Grainger, DW (2013). Developing siRNA therapies to address osteoporosis. *Ther Deliv* **4**: 1239–1246.
19. Zhang, G, Guo, B, Wu, H, Tang, T, Zhang, BT, Zheng, L *et al.* (2012). A delivery system targeting bone formation surfaces to facilitate RNAi-based anabolic therapy. *Nat Med* **18**: 307–314.
20. Liang, C, Guo, B, Wu, H, Shao, N, Li, D, Liu, J *et al.* (2015). Aptamer-functionalized lipid nanoparticles targeting osteoblasts as a novel RNA interference-based bone anabolic strategy. *Nat Med* **21**: 288–294.
21. Chonn, A, Cullis, PR and Devine, DV (1991). The role of surface charge in the activation of the classical and alternative pathways of complement by liposomes. *J Immunol* **146**: 4234–4241.
22. Wei, X, Shao, B, He, Z, Ye, T, Luo, M, Sang, Y *et al.* (2015). Cationic nanocarriers induce cell necrosis through impairment of Na(+)/K(+)-ATPase and cause subsequent inflammatory response. *Cell Res* **25**: 237–253.
23. Li, X, Ominsky, MS, Warmington, KS, Morony, S, Gong, J, Cao, J *et al.* (2009). Sclerostin antibody treatment increases bone formation, bone mass, and bone strength in a rat model of postmenopausal osteoporosis. *J Bone Miner Res* **24**: 578–588.
24. Ominsky, MS, Li, C, Li, X, Tan, HL, Lee, E, Barrero, M *et al.* (2011). Inhibition of sclerostin by monoclonal antibody enhances bone healing and improves bone density and strength of nonfractured bones. *J Bone Miner Res* **26**: 1012–1021.
25. Chen, M, Qiao, H, Su, Z, Li, H, Ping, Q and Zong, L (2014). Emerging therapeutic targets for osteoporosis treatment. *Expert Opin Ther Targets* **18**: 817–831.
26. Li, X, Warmington, KS, Niu, QT, Asuncion, FJ, Barrero, M, Grisanti, M *et al.* (2010). Inhibition of sclerostin by monoclonal antibody increases bone formation, bone mass, and bone strength in aged male rats. *J Bone Miner Res* **25**: 2647–2656.
27. Jayaraman, M, Ansell, SM, Mui, BL, Tam, YK, Chen, J, Du, X *et al.* (2012). Maximizing the potency of siRNA lipid nanoparticles for hepatic gene silencing in vivo. *Angew Chem Int Ed* **51**: 8529–8533.
28. Basha, G, Novobrantseva, TI, Rosin, N, Tam, YY, Hafez, IM, Wong, MK *et al.* (2011). Influence of cationic lipid composition on gene silencing properties of lipid nanoparticle formulations of siRNA in antigen-presenting cells. *Mol Ther* **19**: 2186–2200.
29. Chen, S, Tam, YY, Lin, PJ, Leung, AK, Tam, YK and Cullis, PR (2014). Development of lipid nanoparticle formulations of siRNA for hepatocyte gene silencing following subcutaneous administration. *J Control Release* **196**: 106–112.
30. Mui, BL, Tam, YK, Jayaraman, M, Ansell, SM, Du, X, Tam, YY *et al.* (2013). Influence of polyethylene glycol lipid desorption rates on pharmacokinetics and pharmacodynamics of siRNA lipid nanoparticles. *Mol Ther Nucleic Acids* **2**: e139.
31. Cabral, H, Matsumoto, Y, Mizuno, K, Chen, Q, Murakami, M, Kimura, M *et al.* (2011). Accumulation of sub-100 nm polymeric micelles in poorly permeable tumours depends on size. *Nat Nanotechnol* **6**: 815–823.
32. Huo, S, Ma, H, Huang, K, Liu, J, Wei, T, Jin, S *et al.* (2013). Superior penetration and retention behavior of 50 nm gold nanoparticles in tumors. *Cancer Res* **73**: 319–330.
33. Belliveau, NM, Huft, J, Lin, PJ, Chen, S, Leung, AK, Leaver, TJ *et al.* (2012). Microfluidic synthesis of highly potent limit-size lipid nanoparticles for *in vivo* delivery of siRNA. *Mol Ther Nucleic Acids* **1**: e37.
34. Sahay, G, Querbes, W, Alabi, C, Eltoukhy, A, Sarkar, S, Zurenko, C *et al.* (2013). Efficiency of siRNA delivery by lipid nanoparticles is limited by endocytic recycling. *Nat Biotechnol* **31**: 653–658.
35. Sun, H, Gulbagci, NT, Taneja, R. *Cancer Genomics and Proteomics: Methods and Protocols*. 2007.. P. B. Fisher, edn. Humana Press Inc., Totowa, New Jersey, vol. 383, pp. 311–319.
36. Rettig, GR and Behlke, MA (2012). Progress toward *in vivo* use of siRNAs-II. *Mol Ther* **20**: 483–512.
37. Varghese, F, Bukhari, AB, Malhotra, R and De, A (2014). IHC Profiler: an open source plugin for the quantitative evaluation and automated scoring of immunohistochemistry images of human tissue samples. *PLoS One* **9**: e96801.
38. Burgess, A, Vigneron, S, Brioudes, E, Labbé, JC, Lorca, T and Castro, A (2010). Loss of human Greatwall results in G2 arrest and multiple mitotic defects due to deregulation of the cyclin B-Cdc2/PP2A balance. *Proc Natl Acad Sci USA* **107**: 12564–12569.

Supplementary Information accompanies this paper on the Molecular Therapy–Nucleic Acids website (http://www.nature.com/mtna)